Phase Competition and Weak Hydrogen Bonding in the Giant Hysteresis of an S = 1/2 Nickel Dithiolene Complex: Combined Structural and Magnetic Studies

Olivier Jeannin,[†] Rodolphe Clérac,*[,‡] and Marc Fourmigué*[,§]

Laboratoire Chimie, Ingénierie Moléculaire et Matériaux (CIMMA), UMR 6200 CNRS–Université d'Angers, UFR Sciences, 2 Boulevard Lavoisier, 49045 Angers, France, Université Bordeaux 1, CNRS, Centre de Recherche Paul Pascal–UPR8641, 115 avenue du Dr. A. Schweitzer, 33600 Pessac, France, and Sciences Chimiques de Rennes, UMR 6226 CNRS–Université Rennes 1, Equipe MaCSE, Bât 10C, Campus de Beaulieu, 35042 Rennes cedex, France

Received June 20, 2007. Revised Manuscript Received September 3, 2007

The room-temperature (RT) crystal structure of the colbaltocinium salt of the $S = 1/2$ nickel dithiolene complex $[Ni(tfadt)_2]^{-\bullet}$ (tfadt, 2-trifluoromethylacrylonitrile-1,2-dithiolate) is characterized by uniform one-dimensional spin chains of radical anions, separated from each other by the $[Cp_2Co]^+$ cations. Both entities exhibit disorder affecting one CF_3 and one Cp ring. Upon being cooled from RT (phase A), two successive structural phase transitions lead to tetramerized spins chains with a low-temperature singlet ground state (phase C) with an associated ordering of the CF_3 and Cp moieties. An intermediate tetramerized C′ phase is observed during the cooling sweep, in competition with a dimerized chain structure (phase B) upon warming, affording an apparent giant thermal hysteresis loop of 50 K. The phase succession in temperature at atmospheric pressure is established on the basis of the correlation between the temperature dependence of the magnetic susceptibility and crystal structure data collections and resolutions at seven different temperatures. The behavior of this cobaltocinium salt contrasts strongly with the ferricinium analog, which exhibits successive A ↔ B ↔ C transitions upon being cooled from the regular A phase. A model based on the temperature evolution of the Gibbs energy for the two compounds is proposed to account for those differences. Comparison of the structural data between the salts in the B and C′ phases demonstrates the important role of weak C–H···F,N hydrogen-bond interactions in the stabilization of the different phases depending on the nature of the metallocenium cation.

Introduction

Paramagnetic metal–bis-dithiolene complexes have been widely investigated for their conducting and magnetic properties,[1] and recently, several $[Ni(mnt)_2]^{-\bullet}$ salts were shown to exhibit abrupt paramagnetic–diamagnetic transitions[2] related to spin-Peierls transitions, although their first-order character indicates that such transitions better compare with those described in neutral radical systems such as 1,3,5-trithia-2,4,6-triazapentalenyl (TTTA).[3,4] The absence of hysteresis in those salts, an essential feature for many applications, has urged the elaboration of $[Ni(mnt)_2]^{-\bullet}$ salts with counterion with hydrogen bonding capability,[5,6] in order to increase the intermolecular cooperativity held responsible for wide hysteresis in spin-crossover systems and TTTA radical systems. We have recently described a novel asymmetrically substituted dithiolate ligand, abbreviated as tfadt (2-trifluoromethylacrylonitrile-1,2-dithiolate), which incorporates, in addition to the nitrile moiety found in the mnt dithiolate, a trifluoromethyl group characteristic of the tfd dithiolate ligand.[7]

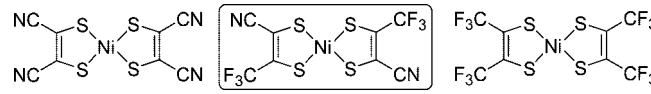

This combination allowed for the preparation of the corresponding square-planar nickel dithiolene complex, $[Ni(tfadt)_2]^{2-,-\bullet}$, both in its closed-shell dianionic and paramagnetic anionic forms. The main differences with $[Ni(mnt)_2]^{-\bullet}$

* Corresponding author. E-mail: clerac@crpp-bordeaux.cnrs.fr (R.C.); marc.fourmigue@univ-rennes1.fr (M.F.).
† Université d'Angers.
‡ Université Bordeaux 1.
§ Université Rennes 1.

(1) *Dithiolene Chemistry: Synthesis, Properties, and Applications*; Progress in Inorganic Chemistry Stiefel,E. I. , Ed.; Wiley: New York, 2003; Vol *52*.
(2) (a) Ren, X.; Meng, Q.; Song, Y.; Hu, C.; Lu, C.; Chen, C.; Xue, Z. *Inorg. Chem.* **2002**, *41*, 5931. (b) Ren, X. M.; Okudera, H.; Kremer, R. K.; Song, Y.; He, C.; Meng, Q. J.; Wu, P. H. *Inorg. Chem.* **2004**, *43*, 2569. (c) Ren, X.; Meng, Q.; Song, Y.; Lu, C.; Hu, C. *Inorg. Chem.* **2002**, *41*, 5686.
(3) Fujita, W.; Awaga, K. *Science* **1999**, *286*, 261.
(4) (a) Brusso, J. L.; Clements, O. P.; Haddon, R. C.; Itkis, M. E.; Leitch, A. A.; Oakley, R. T.; Reed, R. W.; Richardson, J. F. *J. Am. Chem. Soc.* **2004**, *126*, 8256. (b) Barclay, T. M.; Cordes, A. W.; George, N. A.; Haddon, R. C.; Itkis, M. E.; Mashuta, M. S.; Oakley, R. T.; Patenaude, G. W.; Reed, RE. W.; Richardson, J. F.; Zhang, H. *J. Am. Chem. Soc.* **1998**, *120*, 352. (c) Brusso, J. L.; Clements, O. P.; Haddon, R. C.; Itkis, M. E.; Leitch, A. A.; Oakley, R. T.; Reed, R. W.; Richardson, J. F. *J. Am. Chem. Soc.* **2004**, *126*, 14692.
(5) Ren, X. M.; Nishihara, S.; Akutagawa, T.; Noro, S.; Nakamura, T. *Inorg. Chem.* **2006**, *45*, 2229.
(6) (a) Fourmigué, M.; Bertran, J. N. *Chem. Commun.* **2000**, 2111. (b) Fourmigué, M.; Mézière, C.; Dolou, S *Cryst. Growth Des.* **2003**, *3*, 805.
(7) Jeannin, O.; Delaunay, J.; Barrière, F.; Fourmigué, M. *Inorg. Chem.* **2005**, *44*, 9763.

10.1021/cm071652q CCC: $37.00
Published on Web 11/03/2007

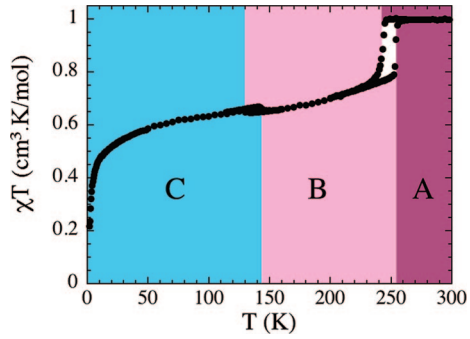

Figure 1. χT vs T plot (where $\chi = M/H$ is the magnetic susceptibility) at 1000 Oe and the different structural phases obtained for $[Cp_2Fe][Ni(tfadt)_2]$ (see ref 9).

are (i) an enhanced stability of the radical anion relatively to the dianion form because the $-CF_3$ moiety is less electron-withdrawing than the –CN one, (ii) a higher solubility in organic solvents, (iii) a disorder of the $-CF_3$ groups on several positions observed in the crystal structures of various salts with PPh_4^+,[7] Bu_4N^+, Et_4N^+,[8] Me_4N^+,[8] and donor molecules such as ferrocene,[9] perylene[10] or bis(ethylenedithio)tetrathiafulvalene (BEDT-TTF).[11] In the solid state, the PPh_4^+ and $^nBu_4N^+$ salts of $[Ni(tfadt)_2]^{-\bullet}$ exhibit a Curie law, as the radical anions are well-separated from each other by the bulky cations.[7] On the other hand, in the Me_4N^+ and Et_4N^+ salts, they stack on top of each other to form spin chains.[8] A second-order phase transition to a singlet ground state was observed at 200 K in the Me_4N^+ salt, where both CF_3 moieties are already ordered above the transition, whereas a first-order phase transition with a 9 K hysteresis was observed at 355–364 K in the temperature dependence of the magnetic susceptibility of the Et_4N^+ salt.[8] This was tentatively attributed to the ordering of one CF_3 group below the phase transition, by comparison with the Me_4N^+ salt that exhibits no such disorder and a second-order phase transition to the singlet ground state. A similar spin chain was also obtained in the ferricinium salt of $[Ni(tfadt)_2]^{-\bullet}$, where both ionic entities are characterized by disorder affecting one CF_3 and one Cp moiety.[9] Above 250 K, this compound displays a Curie-type behavior of noninteracting spins (Phase A). At lower temperatures, not one but two first-order phase transitions, around 249 and 137 K, were revealed by susceptibility measurements with 11 and 16 K hysteresis, respectively. The succession of the structural phases in temperature (Figure 1) was established from crystal structure determinations, showing that the high-temperature transition (phase A ↔ phase B) is associated with an ordering of the CF_3 and Cp groups together with a dimerization of the anionic stacks that thus induces a dramatic drop of the susceptibility. The second low-temperature transition leads to a tetramerization of these nickel dithiolene stacks now in a complete diamagnetic state (phase C), whereas the remaining susceptibility originates from the sole ferricinium contribution.

(8) Jeannin, O.; Clérac, R.; Fourmigué, M *CrystEngComm.* **2007**, *9*, 488.
(9) Jeannin, O.; Clérac, R.; Fourmigué, M *J. Am. Chem. Soc.* **2006**, *108*, 14649.
(10) Jeannin, O.; Fourmigué, M. *New J. Chem.* **2006**, *30*, 1774.
(11) Jeannin, O.; Fourmigué, M. *Inorg. Chim. Acta* **2007**, *360*, 3820.

Scheme 1

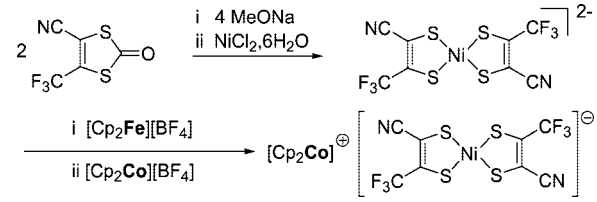

The first-order character of the A ↔ B transition with its associated bistable behavior was thus associated with the structural order–disorder transition,[9] an original behavior in this class of materials in which bistability is most often associated with a strengthening of interstack intermolecular interactions (hydrogen bonding, π–π interactions, etc.).

To investigate these series in more detail, we decided to prepare the analogous cobaltocinium salt, $[Cp_2Co][Ni(tfadt)_2]$, in order to determine if the paramagnetic nature of the ferricinum cation eventually had an influence on the structural and magnetic properties of the nickel dithiolene stacks observed in the structure of $[Cp_2Fe][Ni(tfadt)_2]$. To our surprise and despite an isostructural room-temperature crystal structure, the cobaltocinium salt exhibits a complex behavior with several structural transitions and an apparent 50 K hysteresis as observed by magnetic and X-ray diffraction data. We describe here the complete determination of all the different structural phases present in temperature for the $[Cp_2Co][Ni(tfadt)_2]$ system. Our study has been possible using seven successive X-ray structural determinations at different temperatures combined with magnetic susceptibility measurements, demonstrating that this giant hysteresis results from a subtle competition between two phases in an intermediate temperature regime between 220 and 140 K, associated with the formation of different sets of weak C–H···F,N hydrogen bonds.

Results

Synthesis. The preparation of the $[Ni(tfadt)_2]^{-\bullet}$ nickel complex as n-Bu_4N^+ or PPh_4^+ salt has been described before[7] and involves (Scheme 1) the successive reaction of 4-cyano-5-trifluoromethyl-1,3-dithiole-2-one with (i) MeONa to generate the dithiolate, (ii) $NiCl_2(H_2O)_6$ to form the dianionic complex $[Ni(tfadt)_2]^{2-}$, (iii) n-Bu_4NBr or PPh_4Br to precipitate the salt of the dianion, and (iv) $(Cp_2Fe)(PF_6)$ to oxidize to the monoanioinic $[Ni(tfadt)_2]^{-\bullet}$ species. In the present case, $(Cp_2Co)(PF_6)$ was then added to afford the corresponding colbaltocinium salt through metathesis. Elemental analysis by energy-dispersive X-ray spectroscopy (EDS) showed unambiguously that no residual ferricinium had been left in this cobaltocinium salt (see the Supporting Information).

Room-Temperature X-ray Crystal Structures and Magnetic Behavior. Good-quality crystals of the cobaltocinium analog $[Cp_2Co][Ni(tfadt)_2]$ were obtained by hexane diffusion into a CH_2Cl_2 solution of the title compound. As the ferricinium compound, it crystallizes in the monoclinic system, space group $C2/m$, with both cation and anion located on the mirror plane. This RT phase will be described as phase A in the following discussion. All atoms, except some

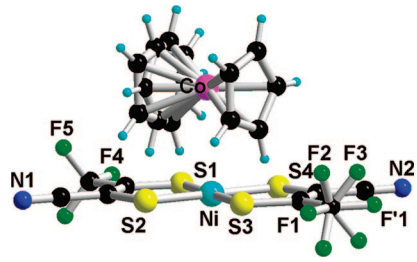

Figure 2. Disorder model of one of the Cp ring and one CF_3 group in $[Cp_2Co][Ni(tfadt)_2]$ at room temperature. Note that the dithiolene complex lies flat on a mirror plane with only F2, F3, and F5 in general position.

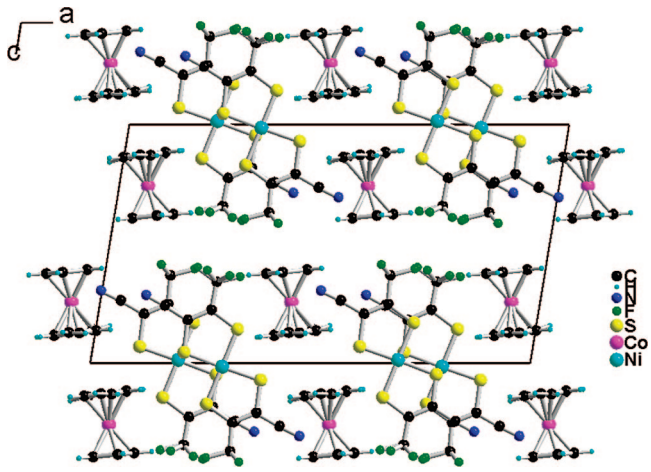

Figure 3. Projection view along *b* of the unit cell of $[Cp_2Co][Ni(tfadt)_2]$ at room temperature (phase A).

fluorine atoms, of the dithiolene complex are located on the crystallographic mirror plane. Furthermore, one of the two CF_3 groups is disordered on two positions related to each other by a 60° rotation (Figure 2). For the $[Cp_2Co]^+$ cation, the mirror plane includes the metal center and one carbon atom of each Cp ring, whereas one of the Cp rings is also disordered on two positions related by a $\pi/5$ rotation (Figure 2).

In the solid state (Figure 3), the dithiolene complexes stack along the *b* axis in a zigzag fashion, and these anionic columns are separated from each other in the *a* direction by dyads of cobaltocenium cations filling pockets between the dithiolene stacks. Within these dyads, the metallocene moieties are organized on top of each other with the disordered Cp rings of both complexes facing each other in a decaled π–π overlap with an intermolecular plane-to-plane distance of 3.375(5) Å.

It is important to note here that the stacks of dithiolene complexes running along *b* are *uniform* stacks, with one single overlap pattern between the radical anions (Figure 3), characterized a large interplanar distance ($b/2 = 3.874$ Å) and by shortest intermolecular Ni···S distance at 3.90 Å and shortest S···S distance at 4.21 Å. Note also that the uniform spin chains of dithiolene radical anions are fully isolated from each other, in the layers by the cobaltocenium cations, in between layers through the nonbonding, soft fluorine–fluorine interface. These large intermolecular distances, combined with the negligible overlap interaction energy between complexes ($\beta = 0.0038$ eV) determined from extended Hückel calculations, indicate that from a magnetic point of view, the radical species are essentially isolated from each other at room temperature. As shown in Figure 4 where the evolution of the χT product has been reported versus the temperature, a temperature-independent χT product is observed at 0.35 cm^3 K mol^{-1} at RT, in accordance with the presence of noninteracting $S = 1/2$ $[Ni(tfadt)_2]^{-\bullet}$ species and diamagnetic $[Cp_2Co]^+$ cations. Besides, we observed that the χT versus T plot strongly differs from that observed in the analogous ferricinium salt reported in Figure 1. It is indeed characterized, by (i) a nonmagnetic ground state in connection with the diamagnetism of the colbaltocinium cation and (ii) an extremely broad and complex thermal hysteresis, as discussed below.

Structural and Magnetic Transitions in $[Cp_2Co]$ Structural and Magnetic Transitions$[Ni(tfadt)_2]$. Upon cooling from room temperature, a first transition is observed at 206 K, which corresponds to a χT decrease from 0.35 to 0.29, leaving 83% of the contribution of the paramagnetic $S = 1/2$ dithiolene complexes. It is followed by a second transition at 149 K, to reach essentially a diamagnetic state. Warming up from this low-temperature phase does not regenerate this intermediate magnetic phase but rather more complicated behavior is observed, with an accident at 163 K and another step around 211 K, before recovering the room-temperature phase. This feature strongly contrasts with that observed in the ferricinium analog (Figure 1) where two "clean" transitions with associated hysteresis were observed. However, a differential scanning calorimetry (DSC) thermogram of $[Cp_2Co][Ni(tfadt_)_2]$ (Figure 5) confirms the presence of only two successive transitions with large enthalpy changes exactly at the temperatures where susceptibility anomalies were also identified during the cooling process (Table 1). Note also that the ΔS values reported in Table 1 (~11–12 J K^{-1} mol^{-1}) exceed the spin-only value for a paramagnetic–diamagnetic transition ($R \ln 2 = 5.76$ J K^{-1} mol^{-1}), indicating that degrees of freedom of the lattice are also involved in the transitions, as indeed observed in the low-temperature X-ray crystal structures (vide infra).

To understand the complex behavior apparently exhibited by this salt, we have performed several X-ray data collections at the important points of the phase diagram, that is at RT, 198 K (↓), 140 K (↓), 170 K (↑), 200 K (↑), 210 K (↑), and RT (↑) again, as shown in Figure 4 with the red ↓ and ↑ arrows indicating that the measurements were performed during the cooling or warming scans, respectively.

At 198 K (↓), below the first transition, a novel crystallographic phase was obtained. The salt crystallizes in the triclinic system, space group $P\bar{1}$ with two crystallographically independent ferricinium cations and two crystallographically independent $[Ni(tfadt)_2]^{-\bullet}$ anions, all of them free of disordered groups (Figure 6). This phase, called C′ in the following, is indeed closely related to the C phase identified at the lowest temperatures in the ferricinium salt.[9] As shown in Figure 6, a projection view along *a*–*c* shows the tetramerized stack consisting of Ni1–Ni2–Ni2–Ni1 moieties. A projection view of the overlap between neighboring com-

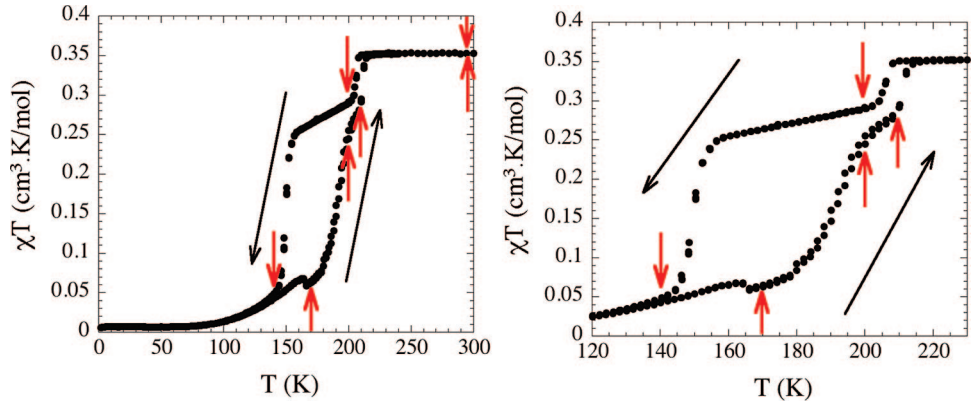

Figure 4. Plots of χT vs T at 1 T and 0.8 K/min for $[Cp_2Co][Ni(tfadt)_2]$ between 1.8 and 300 K (left) and between 120 and 230 K (right). Red arrows indicate the temperatures where X-ray data collections have been performed, during the cooling (RT, 198, and 140 K) and warming scans (170, 200, 210 K, and RT).

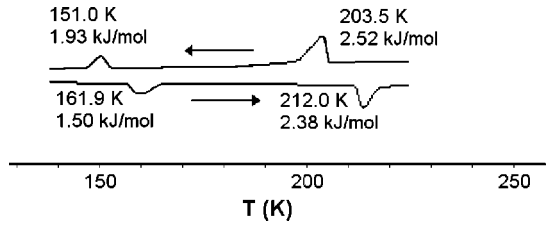

Figure 5. DSC thermogram of $[Cp_2Co][Ni(tfadt)_2]$, with indication of the associated enthalpies (ΔH). Cooling rate 10 K/min, warming rate 5 K/min.

Table 1. Transition Temperatures (T_t), Average Transition Enthalpies (ΔH_t), and Transition Entropies (ΔS_t) for the Two First-Order Transitions in $[Cp_2Co][Ni(tfadt)_2]$

T_t (K)	ΔH_t (kJ mol^{-1})	ΔS_t (J K^{-1} mol^{-1})
207.75	2.45	11.8
156.45	1.71	10.9

plexes (Figure 7), shows indeed that the Ni1–Ni1 interaction is most probably very weak, as confirmed by the calculation of the overlap interaction energies (β) for the three interactions. These values, collected in Table 2, are 0.053, 0.065, and 0.103 eV for the three Ni1–Ni1, Ni1–Ni2, and Ni2–Ni2 interactions, respectively. In this temperature range, these small values are not susceptible to strongly affect the magnetic susceptibility and only the last Ni2–Ni2 interaction (0.10 eV) can be considered to explain the weak decrease of susceptibility observed at 206 K in Figure 4. From a magnetic point of view, this A → C′ transition thus corresponds to a partial dimerization of the uniform spin chain, which would affect only every second dithiolene complex. This behavior contrasts with that observed in the ferricinium salt, where the first transition led to a dimerized system with sizable antiferromagnetic interactions and weak paramagnetism.

A second transition centered around 149 K (Figure 4) abruptly decreases χT down to almost zero, indicating that another structural transition has taken place. Indeed, a third X-ray data collection performed on the same crystal below 149 K, at 140 K, allowed for the identification of the low-temperature C phase, already observed in the ferricinium salt.[9] It is indeed closely related to the C′ phase described above because it crystallizes in the same triclinic space group, $P\bar{1}$, with two crystallographically independent cobaltocinium

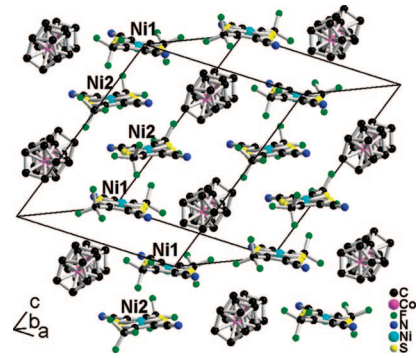

Figure 6. View of $[Cp_2Co][Ni(tfadt)_2]$ at 198 K (phase C′) along the long molecular axis of the dithiolene complexes, showing the organization within the dithiolene stacks.

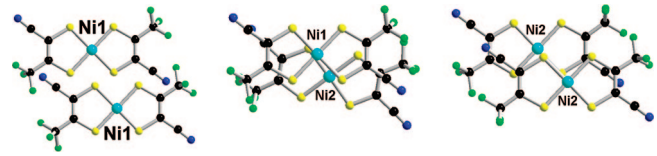

Figure 7. Details of the three overlap patterns in the 198 K structure of $[Cp_2Co][Ni(tfadt)_2]$ (phase C′).

cations and two crystallographically independent $[Ni(tfadt)_2]^{-\bullet}$ anions, all of them free of disordered groups. The main difference with phase C′ lies in the interactions between $[Ni(tfadt)_2]^{-\bullet}$ radical species within the chains. As seen in Table 2, all three Ni1–Ni1, Ni1–Ni2, and Ni2–Ni2 interactions identified above strongly increase in the C phase, up to 0.25 eV for the Ni1–Ni2 overlap. Such a strong overlap, i.e., strong antiferromagnetic interaction, corresponds to a complete depopulation of the triplet state for the Ni1–Ni2 dimeric unit in this temperature range, hence the essentially zero value of the susceptibility in this C phase.

At this stage of our investigation, it is already very surprising that the dimerized B phase identified in the ferricinium salt is not preserved in its colbatocinium analog. The latter thus experiences a A → C′ → C sequence upon cooling, where the C′ phase keeps most of the magnetism of the A phase, at variance with the A → B → C sequence observed in the ferricinium complex, where the B phase was already essentially magnetically silent.

Table 2. Structural Characteristics (Å) and Overlap Energies (eV) of the Three Overlap Patterns in the 198 K↓ (phase C′), 140 K (↓) (phase C), and 210 K (↑) (phase C′) Structures of $[Cp_2Co][Ni(tfadt)_2]$ Together with the Same Data for the Ferricinium Analog at 125 K (↓) in Its Phase C

interaction	interplanar distance	Ni···Ni distance	lateral shift	β (eV)	ref
Ni1–Ni1 @210 K↑ (**Co**, C′)	3.779(4)	5.703(2)	4.27	0.056	this work
Ni1–Ni1 @198 K↓ (**Co**, C′)	3.761(6)	5.729(1)	4.32	0.053	this work
Ni1–Ni1 @140 K↓ (**Co**, C)	3.697(7)	5.811(1)	4.48	0.072	this work
Ni1-Ni1 @125 K↓ (**Fe**, C)	3.735(5)	5.711(3)	4.32	0.109	
Ni1-Ni2 @210 K↑ (**Co**, C′)	[a]	4.317(2)	1.94	0.060	this work
Ni1–Ni2 @198 K↓ (**Co**, C′)	[a]	4.299(1)	1.94	0.065	this work
Ni1–Ni2 @140 K↓ (**Co**, C)	[a]	3.938(1)	1.28	0.252	this work
Ni1–Ni2 @125 K↓ (**Fe**, C)	[a]	3.899(3)	1.19	0.267	
Ni2–Ni2 @210 K↑ (**Co**, C′)	3.636(6)	4.529(2)	2.70	0.103	this work
Ni2–Ni2 @198 K↓ (**Co**, C′)	3.612(7)	4.423(1)	2.72	0.103	this work
Ni2–Ni2 @140 K↓ (**Co**, C)	3.589(7)	4.790(1)	3.17	0.180	this work
Ni2–Ni2 @125 K↓ (**Fe**, C)	3.588(3)	4.785(3)	3.17	0.183	

[a] The dithiolene complexes based on Ni1 and Ni2 are not coplanar.

Table 3. Structural Characteristics (Å) and Overlap Energies (eV) of the Alternated Spin Chain (phase B) of $[Cp_2Co][Ni(tfadt)_2]$ at 170 (↑) and 200 K (↑) and $[Cp_2Fe][Ni(tfadt)_2]$ at 230 K (↑)[a]

interaction	interplanar distance	Ni···Ni distance	lateral shift	β (eV)	α	ref
$[Cp_2Fe][Ni(tfadt)_2]$ (230 K)					0.37	
intradyad	3.705(8)	3.919(2)	1.16	0.248		
interdyad	3.741(8)	5.003(2)	3.36	0.152		
$[Cp_2Co][Ni(tfadt)_2]$ (200 K)					0.28	this work
intradyad	3.695(1)	3.849(2)	1.08	0.294		
interdyad	3.689(1)	5.010(3)	3.39	0.157		
$[Cp_2Co][Ni(tfadt)_2]$ (170 K)					0.21	this work
intradyad	3.681(1)	3.766(2)	0.99	0.355		
interdyad	3.633(1)	5.024(2)	3.42	0.162		

[a] The alternation coefficient α is defined as $(\beta_{inter}/\beta_{intra})^2$.

Upon warming up the crystal from this low temperature diamagnetic C phase, a phase transition was identified on the magnetic susceptibility behavior at 163 K (Figure 4), from a slight sudden decrease of the susceptibility, followed by a continuous increase up to 211 K where another "step" is observed. X-ray data collections were performed within this temperature range between 163 and 211 K, namely at 170 (↑) and 200 K (↑). At those two temperatures, the C phase has transformed into another phase, identified crystallographically as a B phase, since it is isostructural with that already described in the ferriciunum salt.[9] As a consequence, the same dimerized chains of $[Ni(tfadt)_2]^{-\bullet}$ complexes are found, characterized by only two different overlap interactions and their associated calculated energies, β_{intra} and β_{inter}, collected in Table 3. Of particular interest is the evolution of the magnetic alternation of these partially dimerized chains with the temperature. As already mentioned for the ferricinium complex in this B phase, the J and αJ values ($0 < \alpha < 1$) characterizing an alternated chain are directly correlated to the β interactions energies as $\alpha = \alpha J/J = (\beta_{inter}/\beta_{intra})^2$. Comparison in Table 3 of the three B phase structures at three different temperatures, 230 K (↑) for the ferricinium salt and 200(↑) and 170(↑) K for the cobaltocinium salt, shows that upon cooling, the strongest interaction β_{intra} increases with a parallel reinforcement of the alternation. Such a temperature dependence of the alternation parameter, α, is normally associated with second-order spin-Peierls transitions,[12] but also seems to characterize these chains in the B phase.

We are not at the end of this story after three fully characterized phase transitions on a single crystal. Indeed, upon warming this B phase above 200 K, we did not directly recover the original uniform chain at 211 K. A sixth X-ray data collection at 200 K showed the stabilization for the C′ phase, already identified upon cooling the crystal from room temperature. As already shown in Figures 6 and 7, it corresponds to the apparition of two crystallographically independent $[Ni(tfadt)_2]^{-\bullet}$ moieties that are not coplanar anymore and, as a consequence, to the setting of three different intermolecular interactions Ni1–Ni1, Ni1–Ni2, and Ni2–Ni2. The geometrical and energy characteristics of these interactions are collected in Table 2, together with those of phases C′ and C identified upon lowering the temperature to 198 (↓) and 140 K (↓), respectively. Warming up this C′ phase above 211 K to room temperature allowed us to recover the starting A phase that was confirmed by a seventh data collection performed at RT.

Before we discuss all these striking results in detail, it is important to note here the exceptional mechanical strength of the single crystals of this salt, which were able to endure five successive crystallographic transitions ($A_{RT} \rightarrow C' \rightarrow C_{LT} \rightarrow B \rightarrow C' \rightarrow A_{RT}$) with large molecular displacements without losing much of their monocrystalline nature. This was possible only by crossing the phase transitions at a very slow cooling or warming rate (1 K/h) to preserve the integrity of the crystal. Note also that the different phase transitions observed here are not limited to one single crystal, but several crystals were investigated that all showed the same set of phases. Our confidence is also based on the precise correlation between the temperatures deduced from these single-crystal X-ray diffraction studies and the temperatures deduced from the DSC and magnetic susceptibility measurements, which were performed on several milligrams of this compound.

(12) (a) Pincus, P *Solid State Commun.* **1971**, *9*, 1971. (b) Beni, G. *J. Chem. Phys.* **1973**, *58*, 3200. (c) Beni, G.; Pincus, P. *J. Chem. Phys.* **1972**, *57*, 3531.

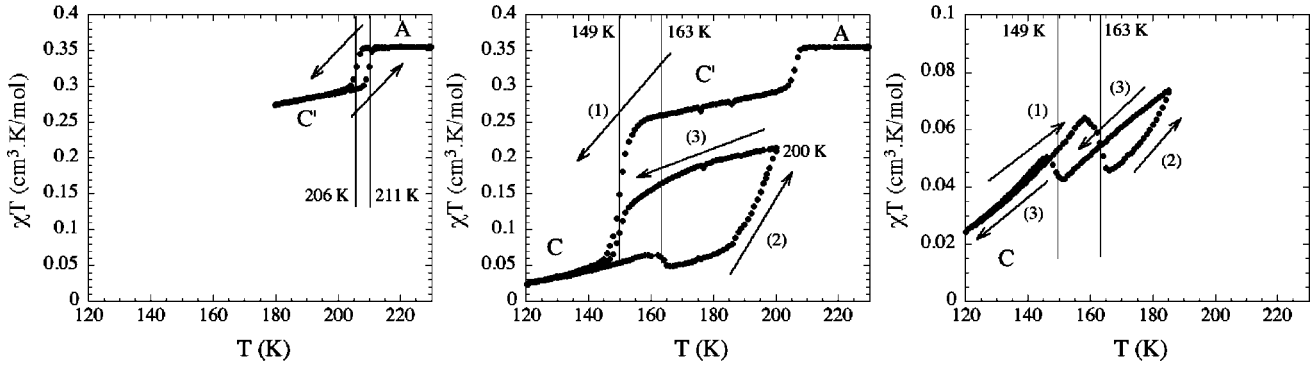

Figure 8. χT s T for $[Cp_2Co][Ni(tfadt)_2]$ at 1 T highlighting the first-order A ↔ C′ transition (left) and (middle and right) the complex hysteresis behavior at the C ↔ B transition.

Discussion

To better understand the striking magnetic and structural behavior of this salt, we have first attempted to separately investigate the two transitions by running small temperature cycles around each of them.

As shown in Figure 8, the first order A ↔ C′ transition is clearly identified by the thermal hysteresis loop observed between 206 and 211 K, confirming the presence of this C′ phase in the warming cycle, as determined from the X-ray data collection performed at (210 K ↑). Minor thermal hysteresis loops have been also performed between the low-temperature C phase and the intermediate phases obtained in the heating mode. As shown in Figure 8 (middle and right), warming from the C phase up to 200 K and then cooling again does not reproduce the same path, and a large hysteresis behavior is again observed with a transition back to the C phase around 149 K. The same type of phenomenon is observed from the C phase when the system is warmed only to 185 K (Figure 8 right).

With our experimental techniques, the B phase has never been detected when decreasing the temperature and it is only possible to obtain this state from the C phase at 165 K in heating mode. This type of behavior is reminiscent of the monotropism observed in polymorphic solids or liquid crystals.[13] In such systems where one observes a series of phase transitions as $\beta \rightarrow \alpha \rightarrow L$ upon warming, the $\beta \leftrightarrow \alpha$ transition is said to be enantiotropic if the intermediate α phase is a thermodynamic one. On the other hand, if the α phase is invariably metastable with respect to β, the $\beta \leftrightarrow \alpha$ transition, when observed, displays a monotropic character. As in these systems, this material present the ability to have two phases, here C′ and B, observed in the same temperature domain even if one of them is naturally the thermodynamic state of the system and the other a metastable phase. Usually, to discriminate between the two phases, one has to compare the transition temperature with the common higher-temperature phase, i.e., the metastable phase having a transition temperature lower than the thermodynamic phase.[13] Here, because the C′ phase is converting in the high-temperature A phase at 211 K, it was not possible to determine a transition temperature between B and A, as the C′ phase always appears before the A phase when increasing the temperature from the B phase. Therefore, it is difficult to establish which one of the B and C′ phase is the thermodynamic one. On the other hand, the appearance of the C′ phase between B and A in the warming mode strongly suggests the thermodynamic nature of the C′ phase. Therefore, on the basis of the experimental data, it is possible to establish a scenario that can be followed on the schematic Gibbs energy versus T diagrams shown on scheme *2*.

Scheme 2. Outlines of the Gibbs energy curves versus temperature for $[Cp_2Co][Ni(tfadt)_2]$ (left) and $[Cp_2Fe][Ni(tfadt)_2]$ (right)

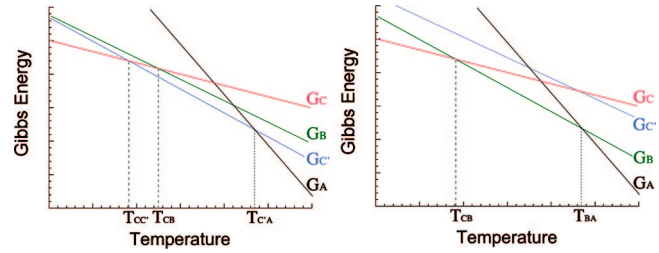

For the cobaltocinium salt (Scheme 2, left), the thermodynamic phases that have the lowest Gibbs energy are C, C′, and A; upon an increase in the temperature, this sequence is changed into C, B, and A in the ferricinium compound. The main difference between the two schemes is the relative energy position of the Gibbs energy of the C′ and B phases. Although these two are relatively well separated in $[Cp_2Fe][Ni(tfadt)_2]$, as suggested experimentally by the two well-defined transitions (C ↔ B and B ↔ A at T_{CB} and T_{BA}, respectively),[9] they seem to be very close in the case of $[Cp_2Co][Ni(tfadt)_2]$, as shown in Scheme 2 (left), although their relative stability is also inversed. This proximity creates the transition temperatures, $T_{CC'}$ and T_{CB}, to be very close. As the C ↔ C′ transition is of first-order nature, the slow dynamics associated with this transition allow, in increasing the temperature, the C phase to convert first and faster in the B metastable phase at T_{CB} (in other words, the system does not have time to wait for the end of the thermal hysteresis loop, i.e., to reach the C → C′ transition, and thus converts first to the metastable B phase). At higher temperatures, kinetic effects are certainly present even if magnetic measurements performed at different sweeping temperature rates (between 0.2 to 1.21 K/min) did not show any

(13) Pardo, L. C.; Barrio, M.; Tamarit, J. L.; Salud, J.; Lopez, D. O.; Negrier, P.; Mondieig, D. *Phys. Chem. Chem. Phys.* **2004**, *6*, 417. (b) Céolin, R.; Agafonov, V.; Louër, D. Dzyabchenko, A.; Toscani, S.; Cense, J. M. *J. Solid State Chem.* **1996**, *122*, 186. (c) Grenberg, J. H. *Mater. Sci. Eng., R* **1996**, *16*, 223.

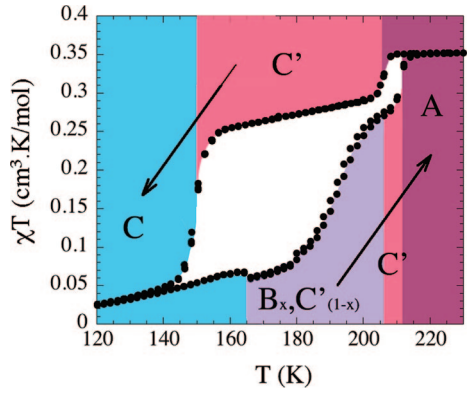

Figure 9. χT vs T plot at 1 T and the different structural phases obtained for $[Cp_2Co][Ni(tfadt)_2]$.

Table 4. Intermolecular C–H···N and C–H···F distances in the A (RT) and the C′ (198 K) phases of $[Cp_2Co][Ni(tfadt)_2]$ as in the B (230 K) phase of $[Cp_2Fe][Ni(tfadt)_2]$[a]

compd	H···N (Å)	C–H···N (deg)	H···F (Å)	C–H···F (deg)
$[Cp_2Co][Ni(tfadt)_2]$	2.50	153	2.71 (×4)	150
phase A at RT			2.64 (×4)	123
$[Cp_2Fe][Ni(tfadt)_2]$	2.67 (×2)	134	2.46 (×2)	130
phase B at 230 K	2.73 (×2)	117	2.56 (×2)	154
			2.70 (× 2)	133
			2.73 (×2)	129
$[Cp_2Co][Ni(tfadt)_2]$	2.44	137	2.54	130
phase C′ at 198 K	2.53	148	2.59	160
	2.55	142	2.61	144
	2.74	135	2.69	164
			2.71	132
			2.79	143
			2.79	120

[a] Only distances below 2.8 Å and with C–H···N,F angles >110° are reported.

significant difference. In this hypothesis, the B phase should very slowly convert into the thermodynamic C′ phase when increasing the temperature between 165 and 200 K, leading to a probable metastable biphasic system: $B_xC'_{(1-x)}$. The presence of both C and B phases in this temperature domain agrees well with the minor hysteresis loops around the C ↔ B transition and shown in Figure 8 (middle and right). Above 200 K, the thermodynamic C′ phase is the only present and thus the compound exhibits the C′ → A transition at $T_{C'A}$. In this scenario, the B phase is not observed when the temperature is decreased as the C′ phase is formed from A faster than the B phase (small hysteresis loop shown in Figure 8, left) around $T_{AC'}$. This might also be the result of a larger difference between G_B and $G_{C'}$ around $T_{C'A}$ than around $T_{CC'}$, as shown in Scheme 2. With this simple hand waving model, it is possible to explain the phase sequences shown in Figure 9 and to suggest that in $[Cp_2Co][Ni(tfadt)_2]$, the C′ phase is now the thermodynamic one whereas the B phase is metastable.

We are now wondering what could be at the origin of the strong differences observed between ferricinium and cobaltocinium salts, and particularly, the different stabilities of the B and C′ phases in the intermediate regime of the cobaltocinium salt. One first point is the paramagnetic nature of the ferricinium ($S = 1/2$), which might have an influence on the regular dimerization process experienced by $[Cp_2Fe][Ni(tfadt)_2]$ whereas the diamagnetic cobaltocinium

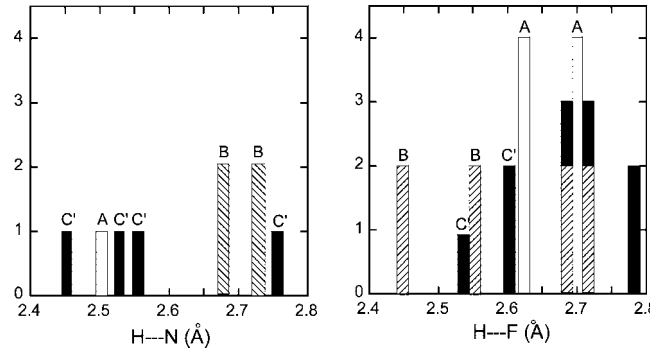

Figure 10. Histograms of (C–)H···N (left) and (C–)H···F (right) short distances in $[Cp_2Fe][Ni(tfadt)_2]$ (phase A at RT and phase B at 230 K) and $[Cp_2Co][Ni(tfadt)_2]$ (phase C′ at 198 K).

salt enters a less-ordered C′ phase upon cooling . This would imply some magnetic interaction between the anionic chains and the ferricinium cations. The crystal structure of the room-temperature A phase does not offer many possibilities in that respect because there is no Cp/dithiolene overlap, which would give rise to a possible direct exchange interaction.

Another rationale for these strikingly different behaviors might be found in the details of weak intermolecular interactions such as C–H···N or C–H···F hydrogen bonds between the hydrogen atoms of the metallocenium cations and the nitrogen or fluorine atoms of the CN and CF_3 groups of the $[Ni(tfadt)_2]^{-\bullet}$ anions. These hydrogen bonds, albeit weak in essence, have been shown to play a crucial role in the organic solid state.[14] Furthermore, despite the fact that the fluorine atoms are poor hydrogen bond acceptors, the hydrogen bond donor character of the cyclopentadienyl ring hydrogen atoms are most probably enhanced in the metallocenium cations. This charge assistance[15] was unambiguously demonstrated by Grepioni and Braga in the course of structural investigations of PF_6^- salts of various metallocenium cations, showing also that the length and number of short (C–)H···F distances correlate with the position of the metal atom in the periodic table, i.e., more numerous and shorter (C–)H···F distances are in the order $Cp_2Fe^+ > Cp_2Co^+$, which is also the order of increasing need of back-donation from the metal atoms onto the ligands.[16] To evaluate if such weak C–H···N,F hydrogen bonds could also play a discriminating role between both salts based on Cp_2Fe^+ and Cp_2Co^+, and particularly between the B and C′ phases in a common temperature range, we have analyzed the occurrence of such weak bonds in the A phases of the two salts, the B phase of the ferricinium, and the C′ phase of the cobaltocinium one (Table 4). The histograms for the C–H···N and C–H···F bonds identified in the different phases are reported in Figure 10.

We observe indeed a notable difference between the B and C′ phases of the ferricinium and cobaltocinium salts,

(14) (a) Desiraju, G. *Acc. Chem. Res.* **1993**, *24*, 290. (b) Gavezzotti, A. *J. Phys. Chem.* **1991**, *95*, 8948. (c) Taylor, R.; Kennard, O. *J. Am. Chem. Soc.* **1982**, *104*, 5063. (d) Desiraju, G. R.; Steiner, T. In *The Weak Hydrogen Bond*; Oxford University Press: Oxford, U.K., 1999.
(15) (a) Braga, D.; Costa, A. L.; Grepioni, F.; Scaccianoce, L.; Tagliavini, E. *Organometallics* **1997**, *16*, 2070. (b) Braga, D.; Angeloni, A.; Grepioni, F.; Tagliavini, E. *J. Chem. Soc., Chem. Commun.* **1997**, 1447.
(16) Grepioni, F.; Cojazzi, G.; Draper, S. M.; Scully, N.; Braga, D. *Organometallics* **1998**, *17*, 296.

Table 5. Crystallographic Data for [Cp_2Co][Ni(tfadt)$_2$] at Different Temperatures in the Thermal Cycle (see text)[a]

	phase						
	A (RT)	C′ (198 K ↓)	C (140 K ↓)	B (170 K ↑)	B (200 K ↑)	C′ (210 K ↑)	A (RT ↑)
formula	$C_{18}H_{10}Co$ $F_6N_2NiS_4$	$C_{18}H_{10}Co$ $F_6N_2NiS_4$	$C_{18}H_{10}Co$ $F_6N_2NiS_4$	$C_{18}H_{10}Co$ $F_6N_2NiS_4$	$C_{18}H_{10}Co$ $F_6N_2NiS_4$	$C_{18}H_{10}Co$ $F_6N_2NiS_4$	$C_{18}H_{10}Co$ $F_6N_2NiS_4$
fw	614.16	614.16	614.16	614.16	614.16	614.16	614.16
cryst syst	monoclinic	triclinic	triclinic	triclinic	triclinic	triclinic	monoclinic
space group	*C*2/*m*	$P\bar{1}$	$P\bar{1}$	$P\bar{1}$	$P\bar{1}$	$P\bar{1}$	*C*2/*m*
a (Å)	23.180(3)	12.3208(14)	12.2269(16)	7.8202(11)	7.859(5)	12.333(2)	23.211(3)
b (Å)	7.7477(5)	12.6666(12)	12.7554(15)	11.5705(18)	11.601(5)	12.6886(18)	7.7363(7)
c (Å)	12.7587(11)	15.3798(16)	14.8842(18)	12.7700(17)	12.792(5)	15.462(2)	12.7856(18)
α (deg)	90.00	82.475(12)	78.428(14)	74.115(17)	74.405(5)	82.416(17)	90.00
β (deg)	99.309(12)	67.071(12)	70.997(14)	82.870(16)	83.095(5)	66.981(17)	99.276(17)
γ (deg)	90.00	80.971(13)	79.285(14)	76.892(17)	76.063(5)	80.951(18)	90.00
V (Å^3)	2261.2(3)	2176.7(4)	2131.9(5)	1080.0(3)	1088.3(9)	2192.7(6)	2265.9(5)
Z	4	4	4	2	2	4	4
d_{calcd}(mg m^{-3})	1.842	1.874	1.914	1.889	1.874	1.860	1.800
diffraction	Stoe-IPDS	Stoe-IPDS	Stoe-IPDS	Stoe-IPDS	Stoe-IPDS	Stoe-IPDS	Stoe-IPDS
temp (K)	293(2)	198(2)	140(2)	170(2)	200(2)	210(2)	293(2)
μ (mm^{-1})	1.996	2.071	2.115	2.087	2.071	2.056	1.989
θ-range (deg)	2.25−25.8	1.65−25.9	1.7−25.75	1.6−25.85	1.6−25.3	1.65−24.5	1.78−25.95
no. of measured reflns	8785	21117	20366	12518	12593	25102	10847
no. of indep. reflns	2344	7813	7612	3887	3916	7854	2339
R_{int}	0.0607	0.0626	0.0803	0.1137	0.1145	0.1206	0.0748
$I > 2\sigma(I)$ reflns	1511	5446	4916	2397	2262	3604	1063
abs corr	multiscan	multiscan	multiscan	Gaussian	Gaussian	Gaussian	Gaussian
T_{max}, T_{min}	0.463, 0.800	0.355, 0.673	0.478, 1.053	0.673, 0.924	0.660, 0.924	0.707, 0.924	0.725, 0.927
no. of refined params	214	577	577	289	289	577	214
$R(F)$, $I > 2\sigma(I)$	0.0457	0.0419	0.0423	0.0651	0.0652	0.0727	0.0423
$wR(F^2)$, all	0.1388	0.1521	0.1402	0.1891	0.1879	0.1988	0.1197
$\Delta\rho$ (e Å^{-3})	+0.51, −0.63	+0.83, −1.16	+1.06, −1.48	+ 0.73, −0.81	+0.72, −0.61	+0.88, −0.60	+0.34, −0.41

[a] The ↓ and ↑ arrows indicate that the data collection has been performed during the cooling or warming sections of the temperature cycle, respectively.

respectively. In the B phase, the shortest intermolecular interactions are of C–H···F type, whereas on the contrary, in the C′ phase, the shortest interactions are C–H···N contacts. This observation strongly suggest that the differential hydrogen-bonding capability of the two metallocenium cations controls here the nature of the structural transitions by modifying the relative stability of the B and C′ phases. Indeed, it should also be recalled that even if the stabilizing energy associated with each individual C–H···F,N contact is probably weak,[14] the cooperative addition of several such contacts brings enough stabilization energy.

Conclusions

We have shown here that the Fe/Co substitution in the metallocenium salts of the paramagnetic [Ni(tfadt)$_2$]$^{-\bullet}$ dithiolene complex induces very strong modifications of their structural and magnetic properties, despite their room temperature isostructural character. The ferricinium salt had been shown to exhibit two successive, well-behaving, first-order phase transitions, from a uniform spin chain (phase A) to a dimerized chain (Phase B) and finally a tetramerized system (Phase C). On the contrary, the cobaltocinium salt prefers to adopt a C′ tetramerized phase upon cooling from RT, before entering the low-temperature C phase. Upon warming, however, a competition between the C′ and B phases leads to an apparent wide hysteresis, which finally ends with the recovery of the C′ phase, before re-entering into the RT A phase. This (B,C′) competition that settles when the system evolves from the low-temperature C phase has been analyzed here by analogy with the monotropic behavior of some substances. In the intermediate temperature range, the B phase of the ferricinium salt is the thermodynamic one and the salt exhibits a kind of polymorphism referred to as enantiotropism, whereas in the cobaltocinium salt, the C′ phase is most probably the thermodynamic one but the salt stabilizes rather in the now-metastable B phase. This work suggest that weak C–H···N,F hydrogen bonds between the Cp rings of the metalloceniums and the –CF_3 and –CN substituents of the dithiolene complex can act as an efficient discriminating tool to favor one or another phase, depending on the nature of the metallocenium cation.

Experimental Section

Syntheses. *[Cp_2Co][Ni(tfadt)$_2$].* Under a nitrogen atmosphere, 4-cyano-5-trifluoromethyl-1,3-dithiole-2-one (0.3 g, 1.42 mmol) is added to a freshly prepared solution of Na (0.07 g, 3 mmol) in dry MeOH (10 mL). The mixture is stirred for 45 min and $NiCl_2(H_2O)_6$ (0.17 g, 0.71 mmol) is added; the red solution is stirred for 20 min and [Cp_2Fe][BF_4] (0.19 g, 0.71 mmol) is added. After 10 min of stirring, [Cp_2Co][BF_4] (0.12 g, 0.71 mmol) is added. After 10 min, water (60 mL) is added, giving a black precipitate that is filtered, dried by suction, and washed with diethyl ether. The precipitate is then dissolved in dichloromethane and precipitated with pentane, filtered, and washed with pentane. The black residue is dissolved in dichloromethane, and the filtered solution is layered with hexane yielding black prisms of the title compound (0.15 g, 0.24 mmol, 34%) suitable for X-ray characterization. Mp: 240 °C. Anal. Calcd for $C_{18}H_{10}F_6N_2S_4Co$ Ni: C, 35.20; H, 1.64; N, 4.56. Found: C, 33.41; H, 1.61; N, 4.59. IR (KBr): υ (cm^{-1}) 2210.83 (C′N). Elemental analysis was also performed by EDS mounted on a JSM 6400 scanning electron microscope (SEM) from Jeol, operating at 20 kV, to check the eventual presence of ferricinium. As shown in the Supporting Information, no trace of iron was identified.

X-ray Data Collection and Structure Refinements. Crystals of [Cp_2Co][Ni(tfadt)$_2$] were mounted at the end of a glass fiber with Araldite glue. The temperature cycle applied to the crystals is

detailed here. Crystal 1: from RT at −50 K/h to 230 K, data collection phase A; cooling down at −20 K/h to 210 K, then at −1K/h to 198 K, data collection phase C′; from 198 at −20 K/h to 165 K, unit cell phase C′, then at −10 K/h to 155 K, then at −1K/h to 140 K (the crystal broke into parts, losing half) data collection phase C; cooling at −10 K/h to 90 K, unit cell phase C. Warming up at −20 K/h to 160 K then at −1 K/h to 170 K, unit cell phase B, crystal explodes. Another crystal was subjected to the whole temperature cycle again, allowing for data collection of the B phase at 170 and 200 K and data collection back at RT as detailed below: from RT at −20 K/h to 210 K, at −1 K/h to 190 K, unit cell phase C′; at −20 K/h to 160 K, at −1 K/h to 140 K, −10 K/h to 130 K, unit cell phase C; +20 K/h to 155 K, +1 K/h to 170 K, data collection phase B, then at +1 K/h to 200 K, data collection phase B, +1 K/h to 207 K, unit cell phase B; +1 K/h to 210 K unit cell phase C′; +1 K/h to RT, data collection phase A.

Data were collected on a Stoe imaging plate diffraction system (IPDS) with graphite-monochromated Mo Kα radiation (λ = 0.71073 Å). The crystal data are summarized in Table 5. Structures were solved by direct methods (SHELXS-97) and refined (SHELXL-97) by full matrix least-squares methods. Absorption corrections were applied for all structures. Hydrogen atoms were introduced at calculated positions (riding model), included in structure factor calculations, and not refined. Disorder models were used in the room temperature structure (phase A) for one CF_3 and one Cp moieties (see text). Refinement of occupation parameters led to an approximate 50:50 distribution. This value was then fixed at 50:50 and not refined any more.

Magnetic Measurements. The magnetic susceptibility measurements were obtained with the use of a Quantum Design SQUID magnetometer MPMS-XL. This magnetometer works between 1.8 and 400 K for dc applied fields ranging from −7 to 7 T. Measurements were performed on polycrystalline samples of $[Cp_2Co][Ni(tfadt)_2]$ (51.19 mg). *M* versus *H* measurements have been performed at 100 K to check for the presence of ferromagnetic impurities that has been found absent. The magnetic data were corrected for the sample holder and the diamagnetic contribution.

Acknowledgment. Financial support from the Ministry of Education and Research (France) to O.J. is gratefully acknowledged. We thank S. Casale from the CMEBA (Rennes) for the EDS experiments. R.C. thanks MAGMANet (NMP3-CT-2005-515767), the CNRS, the University of Bordeaux 1, and the Conseil Régional d'Aquitaine for financial support.

Supporting Information Available: Comparison of EDS analyses for the ferricinium and cobaltocinium phases (PDF); crystallographic information in CIF format. This material is available free of charge via the Internet at http://pubs.acs.org.

CM071652Q